Journal of Wasit for Science and Medicine 2023: 16 (3), 84-93

Synthesis, Structural, and Morphology of Zinc Sulfide Thin Film Nanoparticle Annealing

Aqeel Abdul Jaleel Ali

Ministry of Education, General Directorate of Education in Al-Diwaniyah Governorate, Iraq

Abstract

An electrochemical process was used to deposit zinc sulfide thin films on glass substrates. The study aims to determine whether the annealing of zinc sulfide thin films changes their properties. An analysis of the X-ray diffraction patterns (XRD) determined that annealing controls zinc sulfide (ZnS) thin-film crystallinity and influences the structure of zinc sulfide crystallites, which range from cubic to hexagonal. A Field Emission Scanning Electron Microscope was used (FESEM) to obtain images of thin films. None of thin films that not paneled or annealed displayed grain-like morphologies. while grain growth was an appropriate response to annealing at 150, 250 or 350 °C. Distributed crystalline quality, the EDX analysis confirms the presence of zinc and sulfur in the obtained films, distributed crystalline quality.

Keywords: Nanostructured, Nanoparticle, Zinc Sulfide Thin Films, Annealing, morphology.

1 Introduction

Nanostructured semiconductors have recently been applied to enhance the showing of various systems, including photocatalysts, optical sensors, and solar cells. Zinc sulfide (ZnS) nanostructures are being studied for a broad range of applications [1]. The compound semiconductors IV-VI include zinc sulfide (ZnS), which is a metal chalcogenide. At room temperature, this semiconductor material consists mainly of a cubic phase (zinc blend). At higher temperatures, the structure is hexagonal (quartzite). In the cubic and quartzite phases, the band gap energies are respectively 3.68 eV, and 3.77 eV. The band gap provides a supporting evident that ZnS exhibits a wide band gap [2]. As with III-nitrides and their alloys [3, 4]. The wide band-gap material possesses

properties that make it very beneficial for LEDs, cathodic-ray tubes, sensors, lasers, and solar cells [5-6]. Moreover, ZnS is widely used in, sensors, biological, light-emitting diodes (LEDs), and solar cell applications [7-9]. Zinc sulfide shows a high refractive index (n) at room temperature, high price, and nontoxic properties, among other characteristics [10]. Several methods for synthesizing ZnS have been developed, including chemical bath deposition [11], sol-gel [12], vacuum evaporation [13, 14], electrochemical deposition [15], and spray pyrolysis [16]. Its cost-effectiveness and ease of control make electrodeposition the method of choice among these methods [17]. The effect of various annealing parameters on ZnS thin films were studied by many researchers. Mezan and co-workers reported that at 400 °C, the cubic ZnS phase transformed into a hexagonal structure [18]. While, raising the annealing temperature of ZnS from 100 to 500 °C. On the other hand, Hamzah et al. [19] found that their crystallite size was increased, and their band gap energy decreased. Moreover, zinc sulfide's optical and structural properties are also enhanced by annealing [19]. Zinc sulfide thin films were annealed at temperatures between 350 and 500 °C.

However, increasing the annealing temperature increases the optical transmittance of the films from 65 % to more than 85 % within the visible spectrum [19]. The application of different annealing conditions to thin zinc sulfide films were reported extensively before [20]. The light transmitted by ZnS is more energetic because of its wider band gap in comparison with CdS. The emission in the visible range is enhanced by passing photons through the absorbing layer of the junction. As a result, ZnS buffer layers are an alternative to the chemically deposited CdS in CIGS solar cells [20-22]. Because ZnS layers are inexpensive, non-toxic, and can be grown through multiple methods. These methods include chemical solar synthesis, chemical bath deposition, co-precipitation method, colloidal method, evaporation, and sputtering. The Co-precipitation method is one of the most cost-effective deposition techniques because Co-precipitation uses spin coating to synthesize and deposit. In this study, the structural and morphological properties of zinc sulfide were studied, which we can benefit from in several applications such as solar cells.

2 Experimental

2.1 Unannealed and annealed films of ZnS

Three-electrode electrochemical deposition process was used to synthesize zinc sulfide thin films in this study. Saturated calomel electrodes (SCE) and platinum wire served as electrodes. Samsung electrolyte consisted of $Na_2S_2O_3.5H_2O$ (1 M) and $ZnCl_2.2H_2O$ (1M) in an aqueous solution. The deposition conditions of the samples were not different. Deposition potential, deposition time, and bath temperature were four ranges corresponding to pH 2.8, at 1.0 V, 25 during minutes, and at 30 ℃ respectively. A potentiostat/galvanostat was used to control the deposition potential (Autolab, A3ut 71167, and the Netherlands).

Following deposition, the thin films were removed from the bath, and washed gently with deionized water, and dried. A series of 35, 65-95 minutes anneals were performed on the zinc sulfide thin films that obtained at 150, 250, or 350 ℃ under nitrogen atmosphere. Moreover, temperatures of ambient substrates were observed and stabilized before deposition at 25 ℃. Once deposited at the correct temperature, the ZnS was recorded and deposited at 25 degrees Celsius. source materials were slowly heated up by reproducible the current of the crucible heater. When the deposition rate of 0.50 nm/s was done and stabled at + 0.05 nm/s, the hemistich was opened. Depositions were neatly utter using the same parameters until a thickness of 0.4.5 µm was obtained.

2.2 Instrumentation

Zinc sulfide thin films were characterized by powder X-ray analysis to determine their structural and phase characteristics. Furthermore, molecular composition, and morphological characteristics (FESEM) were used to study the resulted ZnS samples. Energy dispersive spectroscopy (EDS), FESEM (TE SCAN), UV-Vis (Lambda 25-600) and photoluminescence (PL; Renishaw) were also used to test the optical properties.

3. Result and Discussion

3.1 XRD Analysis

The XRD patterns as shown in (figure 1) illustrates the underlying XRD patterns for thin films of ZnS annealed under different conditions and the XRD analysis for an unpaneled sample. A single sharp peak is seen at 26 ° to 27 ° on the XRD spectrum of the unpaneled zinc sulfide. ZnS thin film particles along the

preferred plane when nucleation and growth occur along this plane. In addition, this peak indicates the orientation of the (111) plane of cubic zinc sulfide of the sample that has not been annealed. However, the XRD of the annealed thin films includes a few distinct peaks because of the annealing procedures. In both cases, the peaks are located at 30 °, with the corresponding crystallographic plane being (111).

A hexagonal ZnS crystallite is present in this sample (standard card number 00-039-1363). At higher temperatures, ZnS forms the hexagonal phase. As a result, as annealing time, and temperature increase, during this period, the hexagonal ZnS peak intensity increases, and the cubic ZnS peak intensity decreases. The intensity of the annealing process will increase if the annealing time is elevated from 35 to 95 minutes. Also, to estimate the crystallite average size of the zinc sulfide films, Scherrer's equation was used as shown in equation one and (table 1).

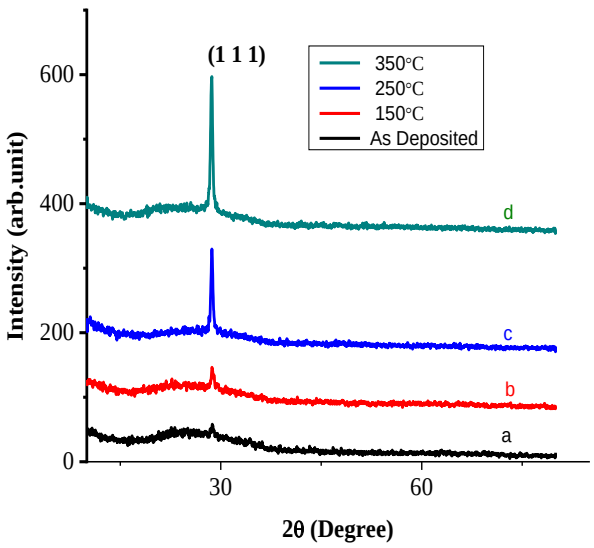

Figure 1: Powder XRD patterns for (a) as deposited and annealed zinc sulfide nanoparticle. (b) The thin film at 150 °C. (c). The material at 250 °C, and (d) the material at 350 °C.

Table1: Structural properties and crystallite sizes of zinc sulfide films as-deposited and annealed at different temperatures based on equation one $D_{hkl} = \frac{k\lambda}{\beta cos\theta}$ (1).

ZnS Thin Film	2Θ	FWHM	d-Spacing	Crystal size D (nm)	
As deposited	26.8	0.3961	3.23	27	
150 °C		26.7	0.5852	3.33	16
250 °C		27.6	0.3735	3.53	13
350 °C		27.4	0.5985	3.24	12

3.2 Surface Morphology

As-deposited film topography is illustrated in (figure 2) the film and the

blister-like particles are homogeneously distributed and of no uniform, sizes ranging from tens of nanometers to approximately 250 nm. Besides, (figure 3) shows an awl-like structure with sizes from 15 to 18 nanometers in spherical nanosized grains of the globule-like structure. The grains are tightly packed together to form a crystalline matrix. Moreover, (figure 3) displays the entire corresponding area more specifically the cross-sectional, and surface features.

After annelation the thin films, size variation of the resulted particles was reduced, and the resulted particles were more uniform. Moreover, (figure 4) illustrate the annealing temperature at 250 °C and shows that specific areas of the crystalline surface features become pebble-like in size and ranging from 13 to 14.5 nm. However, the blister-like features in (figure 4) generate crystalline features as temperature increases through surface diffusion and volume diffusion, respectively. Figure 5 shows the annealed film SEM micrographs at 350 °C, as the broad area is noticed clearly. Figure 5 also shows a dramatic change in crystalline structural features in comparison with the 150 °C annealing temperature in (figure 3).

For a thin film synthesis, excellent single-crystalline structures grown up to 1 mm in width with polygon-like [20-23]. Faces exist, but their number is lower than the required crystalline voids. Although the surface of the film is covered in crystals and has pores, the grain boundary lines appear to demarcate crystalline grain boundaries and are clearly visible. Grains range from 12 to 30 nanometers were discovered on top surfaces of the embedded crystalline grains form a mosaic pattern and visually appealing. while crystals or smaller grains were heated, they diffuse and coalesce to produce larger crystalline grains with distinct crystallographic faces. The annealing process produces two parallel grain growth processes.

The first grain growth process shows three steps, the first step located within the thin film matrix. While the second is located over the thin film matrix, and the third occurring over the thin film surface during the annealing process, as one side of crystals on the surface and pores. The secondary growth process on the film's surface SEM cross-sectional imaging revealed that the resulted films were approximately 4 mm thickness and, also shows that thin films annealed at different temperatures are nonstoichiometric in nature.

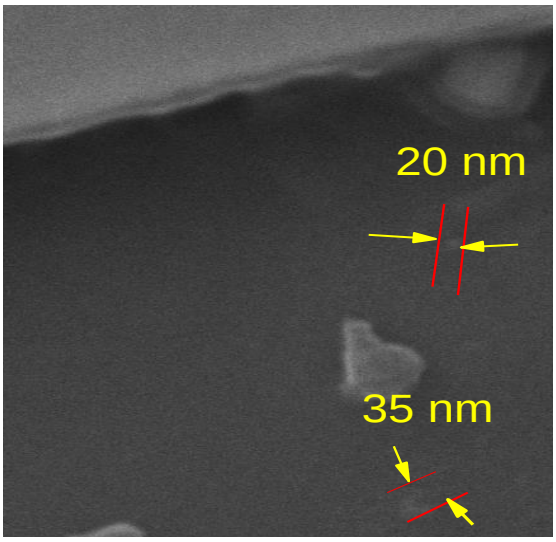

Figure 2: FESEM image of ZnS nanoparticles as deposited.

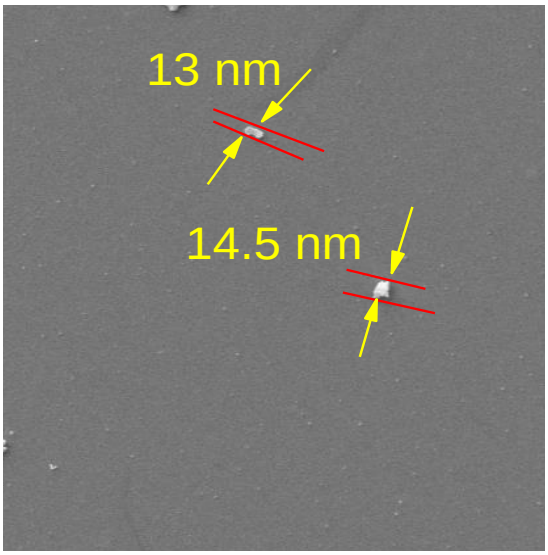

Figure 4: FESEM image of ZnS nanoparticles at 250 °C.

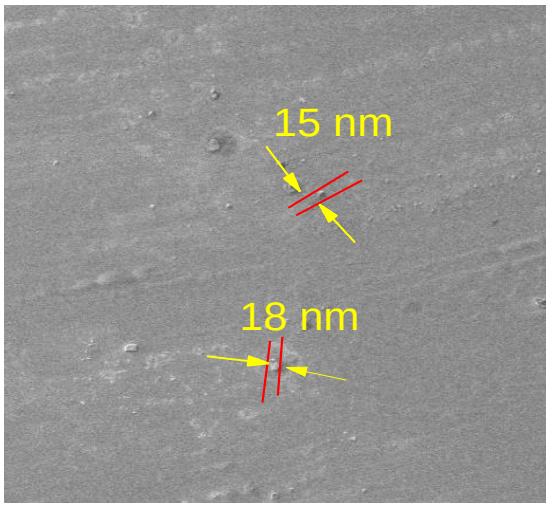

Figure 3: FESEM image of ZnS nanoparticles at 150 °C.

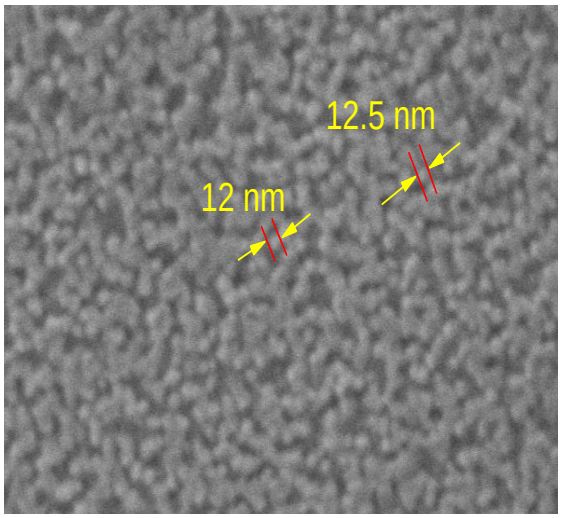

Figure 5: FESEM image of ZnS nanoparticles at 350 °C.

3.3 EDS analysis

Elemental composition of the resulted materials was determined by EDS analysis. The results of EDS spectroscopy on a thin film of ZnS deposited as-deposited

is shown in (figure 6). While the occurrence of Zn and S in the thin film confirms its successful formation in (table 2). Other peaks for example Si, O, and Mg represent the glass substrate applied to the sample. Finally, these spectra do not exhibit an impurity peak.

Table 2: The elemental composition of ZnS materials.

Element	Weight %	Atomic %
S	29.09	40.73
Zn	70.91	59.27
Total	100	

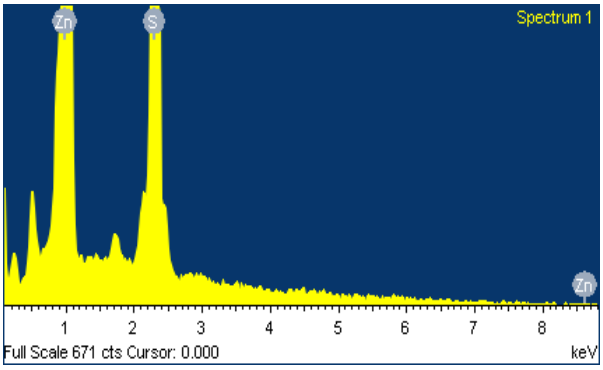

Figure 6: EDS spectra of ZnS as-deposited compound.

4 Conclusion

In conclusion this study involved the use of electrodeposited ZnS nanoparticles thin films, to investigates the impact of annealing conditions on ZnS nanoparticle's structure, and morphology. Different annealing times and temperatures were used to anneal the as-deposited ZnS sample. An XRD pattern revealed that the ZnS sample unannealed was composed of cubic crystals, whereas annealed samples contained hexagonal crystals. Additionally, the XRD results showed that annealing increased this crystallite's size and decreased the strain as well as the hexagonal arrangement of that crystal lattice. Using the FESEM technique, the research determined the morphological characteristics of resulted samples that all have a grainy morphology.

5 References

1. Hajimazdarani M., Ghasali E., Naderi N., and Orooji, Y., (2020). Enhanced optical properties and photodetection behavior of ZnS thin film deposited by electron beam evaporation upon doping with europium oxide. Ceramics International. 46, 18, 28382-28389.
2. Mezan S. O., Jabbar A. H., Hamzah M. Q., Tuama A. N., Hasan N. N., and Agam M. A., (2018). Synthesis and Characterization of Zinc Sulphide (ZnS) Thin Film Nanoparticle for Optical Properties. Journal of Global Pharma Technology. 10, 7, 369-373.

3. Karim A. H., Ali A., and Mezan S., (2021). Synthesis and Characterization of Silica Nanoparticle (SiO_2 Nps) Via Chemical Process. Annals of the Romanian Society for Cell Biology. 25, 6, 6211-6218.
4. Nanda J., Sapra S., and Sarma D. D., Chandrasekharan N., and Hodes G., (2000). Size-selected zinc sulfide nanocrystallites: synthesis, structure, and optical studies. Chemistry of Materials. 12, 4, 1018-1024.
5. Kamel A. A. K., Hussein A. T. A., Shekban A. H., Badr N. R., Mezan S. O., and Jabir W. Q., (2021). Improvement of a New Analysis Technique of phenomenon of bulling and Cyberbullying among Students at different stages. Turkish Journal of Computer and Mathematics Education. 12, 7, 3106-3115.
6. Mezan, S. O., (2021). Silica/Polystyrene Nanocomposite (SiO_2/PsNCs) using Sol-Gel Method Drug Delivery System: A Review. Design Engineering. 10175-10181.
7. Hajimazdarani M., Naderi N., and Yarmand B., (2019). Effect of temperature-dependent phase transformation on UV detection properties of zinc sulfide nanocrystals. Materials Research Express. 6, 8, 085096.
8. Mezan, S. O., Jabbar A. H., Hamzah M. Q., Tuama A. N., Hasan N. N., Roslan M. S., and Agam M. A., (2019). Synthesis, characterization, and properties of polystyrene/SiO_2 nanocomposite via sol-gel process. In AIP Conference Proceedings. 2151, 1, 020034.
9. Mezan S. O., Al Absi S. M., Jabbar A. H., Roslan M. S., Agam M. A., (2021). Synthesis and characterization of enhanced silica nanoparticle (SiO_2) prepared from rice husk ash immobilized of 3-(chloropropyl) triethoxysilanea. Materials Today: Proceedings. 42, 5, 2464-2468.
10. Choudapur V. H., Kapatkar S. B., and Raju A. B., (2019). Structural and optoelectronic properties of zinc sulfide thin films synthesized by Co-precipitation method. ACTA CHEMICA IAŞI. 27, 2, 287-302.
11. Turki J. A., Hussain D. S., Oudah M. S., Aravindhan S., Kadhim M., and Aljeboree M. A., (2021). CuO/ZrO_2 nanocomposites: facile synthesis,

characterization, and photocatalytic degradation of tetracycline antibiotic. Journal of Nanostructures. 11, 2, 333-346.

12. Maseer M. M., Alnaimi F. B. I., Hannun R. M., Wai L. C., Al-Gburi K. A. H., and Mezan S. O., (2022). A review of the characters of nanofluids used in the cooling of a photovoltaic -thermal collector. Materials Today: Proceedings. 57, 2, 329-336.
13. Padmavathy V., Sankar S., and Ponnuswamy V. (2018). Influence of thiourea on the synthesis and characterization of chemically deposited nano structured zinc sulphide thin films. Journal of Materials Science: Materials in Electronics. 29, 9, 7739-7749.
14. Al Absi S. M., Jabbar A. H., Mezan S. O., Al-Rawi B. A., Al-Attabi S. T., (2021). An experimental test of the performance enhancement of a Savonius turbine by modifying the inner surface of a blade, Materials Today: Proceedings. 42, 5, 2233-2240.
15. Jabbar A. H., Mezan S. O., Al Absi S. M., Agam M. A., (2021). Assessment of anticholinesterase effect of polyvinylpyrrolidone/silver nanocomposite biosynthesized by Pandanus Artocarpus extract. Materials Today: Proceedings. 42, 5, 2578-2583.
16. Whyte S., Ogbuefi U. C., Daniel-Mkpume C. C., Anyaka B. O., Okorie B. A., and Ezema F. I., (2020). The influence of substrate temperature on properties of zinc sulphide thin films synthesized by chemical spray pyrolysis. Asian Journal of Basic Science and Research (AJBSR). 2, 1, 1-15.
17. Altajer A. H, Amri T. F., Hasan J. A., Mezan S. O., Thangavelu L., Kadhim M. M., and Alkaim A. F., (2021). Novel Carbon Quantum Dots: Green and Facile Synthesis, Characterization and its Application in On-off-on Fluorescent Probes for Ascorbic Acid. Journal of Nanostructure. 11, 2, 236-242.
18. Mezan, S. O., Jabbar, A. H, Al Absi S. M., Roslan M. S., and Agam M. A., (2021). Synthesis and enhancement of morphological and structural properties of zinc sulphide thin films nanoparticle for solar cell application. In AIP Conference Proceedings. 2398, 1.

19. Hamzah M. Q., Jabbar A. H., Mezan S. O., Tuama A. N., and Agam M. A., (2019). Fabrications of PS/TiO_2 nanocomposite for solar cells applications. In AIP Conference Proceedings. 2151, 1, 020011. AIP Publishing LLC.
20. Tuama A. N., Abbas K. H., Hamzah M. Q., Jabbar A. H., and Agam M. A., (2020). An Overview on Characterization of Silver/Cuprous Oxide Nanometallic (Ag/Cu_2O) As Visible Light Photocatalytic. International Journal of Advanced Science and Technology. 29, 3, 5008-5018.
21. Mezan S. O., Hello K. M., Jabbar A. H., Hamzah M. Q., Tuama A. N., Roslan M. S., and Agam, M. A., (2020). Synthesis and Characterization of Enhanced Polyaniline Nanoparticles by Oxidizing Polymerization. Solid State Technology. 63, 1, 256-266.
22. Nikzad M., Khanlary M. R., and Rafiee S., (2019). Structural, optical, and morphological properties of Cu-doped ZnS thin films synthesized by sol–gel method. Applied Physics A. 125, 8, 1-9.